



TRANSLATIONAL RESEARCH PAPER



DIRAS3 induces autophagy and enhances sensitivity to anti-autophagic therapy in KRAS-driven pancreatic and ovarian carcinomas

Gamze Bildik ^a, Joshua P. Gray^a, Weiqun Mao^a, Hailing Yang^a, Rumeysa Ozyurt^a, Vivian R. Orellana^a, Olivier De Wever^b, Mark S. Carey^c, Robert C. Bast, Jr^a, and Zhen Lu ^a

^aDepartment of Experimental Therapeutics, The University of Texas MD Anderson Cancer Center, Houston, TX, USA; ^bLaboratory of Experimental Cancer Research, Cancer Research Institute Ghent, Belgium; Department of Human Structure and Repair, Ghent University, Ghent, Belgium; ^cDepartment of Obstetrics and Gynecology, University of British Columbia, Vancouver, BC, Canada

ABSTRACT

Pancreatic ductal adenocarcinoma (PDAC) and low-grade ovarian cancer (LGSOC) are characterized by the prevalence of KRAS oncogene mutations. DIRAS3 is the first endogenous non-RAS protein that heterodimerizes with RAS, disrupts RAS clustering, blocks RAS signaling, and inhibits cancer cell growth. Here, we found that DIRAS3-mediated KRAS inhibition induces ROS-mediated apoptosis in PDAC and LGSOC cells with KRAS mutations, but not in cells with wild-type KRAS, by downregulating NFE2L2/Nrf2 transcription, reducing antioxidants, and inducing oxidative stress. DIRAS3 also induces cytoprotective macroautophagy/autophagy that may protect mutant KRAS cancer cells from oxidative stress, by inhibiting mutant KRAS, activating the STK11/LKB1-PRKAA/AMPK pathway, increasing lysosomal CDKN1B/p27 localization, and inducing autophagic gene expression. Treatment with chloroquine or the novel dimeric chloroquine analog DC661 significantly enhances DIRAS3-mediated inhibition of mutant KRAS tumor cell growth in vitro and in vivo. Taken together, our study demonstrates that DIRAS3 plays a critical role in regulating mutant KRAS-driven oncogenesis in PDAC and LGSOC.

Abbreviations: AFR: autophagic flux reporter; ATG: autophagy related; CQ: chloroquine; DCFDA: 2'-7'-dichlorodihydrofluorescein diacetate; DIRAS3: DIRAS family GTPase 3; DOX: doxycycline; KRAS: KRAS proto-oncogene, LGSOC: low-grade serous ovarian cancer; MiT/TFE: microphthalmia family of transcription factors; NAC: N-acetylcysteine; PDAC: pancreatic ductal adenocarcinoma; ROS: reactive oxygen species; TFEB: transcription factor EB

ARTICLE HISTORY

Received 12 April 2023
Revised 6 December 2023
Accepted 20 December 2023

KEYWORDS


Autophagy; chloroquine; DIRAS3; KRAS; LGSOC; PDAC

Introduction

The RAS family of proto-oncogenes, including KRAS, NRAS, and HRAS are GTPases localized in the cell membrane that regulate cell proliferation, motility, and apoptosis [1–3]. Among these, KRAS is the most frequently mutated RAS isoform, and its mutational activation is the critical genetic driver of several cancers, including 95% of pancreatic ductal adenocarcinomas (PDAC) and up to 40% of low-grade serous ovarian cancers (LGSOC) [4,5]. In addition to promoting cell growth and division, mutant KRAS can also stimulate mechanisms such as autophagy [6,7]. Recent studies have shown that KRAS mutant (G12C and G12D) tumors are dependent on autophagy for survival when the KRAS pathway is inhibited [8,9]. Furthermore, cancer cells with KRAS mutations can be eliminated by simultaneous inhibition of both MAP2K/MEK or MAPK/ERK kinases and autophagy in PDAC with evidence of clinical benefit [8,9]. However, the precise molecular mechanism underlying cancer cell death by inhibiting both mutant KRAS signaling and autophagy remains largely unknown. Our group has previously discovered the tumor suppressor protein DIRAS3/ARHI which is

the first endogenous non-RAS protein known to inhibit RAS function by directly binding to KRAS with high affinity. This binding inhibits KRAS dimerization/nanoclustering, blocks effector activation, and reduces cancer cell growth [10]. Here, we further demonstrate that DIRAS3-mediated inhibition of KRAS induces ROS-mediated apoptosis in PDAC and LGSOC cell lines with different KRAS mutations. This is achieved by downregulating the NFE2L2/Nrf2 transcriptional program, reducing antioxidants, and inducing oxidative stress. Interestingly, we also have shown that DIRAS3 inhibition of KRAS elevated the already high basal levels of autophagy in PDAC and LGSOC, while inducing cytoprotective autophagic flux in cell lines with different RAS mutations, but not in the cancer cell lines with wild-type (WT) KRAS. Additionally, our study shows that DIRAS3 inhibits mutant KRAS signaling by activating the STK11/LKB1-AMPK pathway, increasing lysosomal CDKN1B/p27 localization, and activating the MiT/TFE transcriptional program, which in turn increases transcription of autophagy-related genes. Importantly, treatment with autophagy inhibitors chloroquine or the novel dimeric chloroquine analog DC661 significantly

CONTACT Zhen Lu  zlu@mdanderson.org; Robert C. Bast  rbast@mdanderson.org  Department of Experimental Therapeutics, The University of Texas MD Anderson Cancer Center, 1901 East Rd, Houston, TX 77054, USA
Zhen Lu and Robert C. Bast, Jr. who contributed equally to this project.

 Supplemental data for this article can be accessed online at <https://doi.org/10.1080/15548627.2023.2299516>

enhances DIRAS3-mediated inhibition of mutant KRAS signaling and tumor growth in vitro and in vivo. These inhibitors disrupt the oxidant/antioxidant balance through the SQSTM1/p62-KEAP1 pathway, prevent ROS clearance, and enhance cytotoxicity and apoptosis.

Results

DIRAS3 expression decreases RAS-MAP2K/MEK-MAPK/ERK signaling and inhibits cancer cell growth in pancreatic ductal adenocarcinoma (PDAC) and ovarian cancer cell lines driven by different KRAS mutations, but not in PDAC and ovarian cancer cell lines with WT KRAS

DIRAS3 inhibits cancer cell growth by blocking KRAS dimerization and decreasing RAS-MAP2K/MEK-MAPK/ERK

signaling in PDAC and ovarian cancer cell lines and xenografts [10]. The activity of several FDA-approved drugs that inhibit KRAS directly is restricted to particular KRAS mutations. Consequently, we asked whether the expression of DIRAS3 can inhibit cancer cell growth driven by several different KRAS mutations and whether cancers with WT KRAS might not be affected. To measure DIRAS3's effect on KRAS signaling, we established inducible expression of DIRAS3 in 9 PDAC and ovarian cancer cell lines with either mutant or WT KRAS. Using phosphorylation of MAPK/ERK (p-MAPK/ERK) as a target, we found that doxycycline (DOX)-induced DIRAS3 expression significantly decreased p-MAPK/ERK in all 7 PDAC and ovarian cancer cell lines with mutant KRAS regardless of the type of KRAS mutation, but not in the cell lines with WT KRAS (Figure 1A). Interestingly, the BxPC-3-DIRAS3 cell line, which harbors

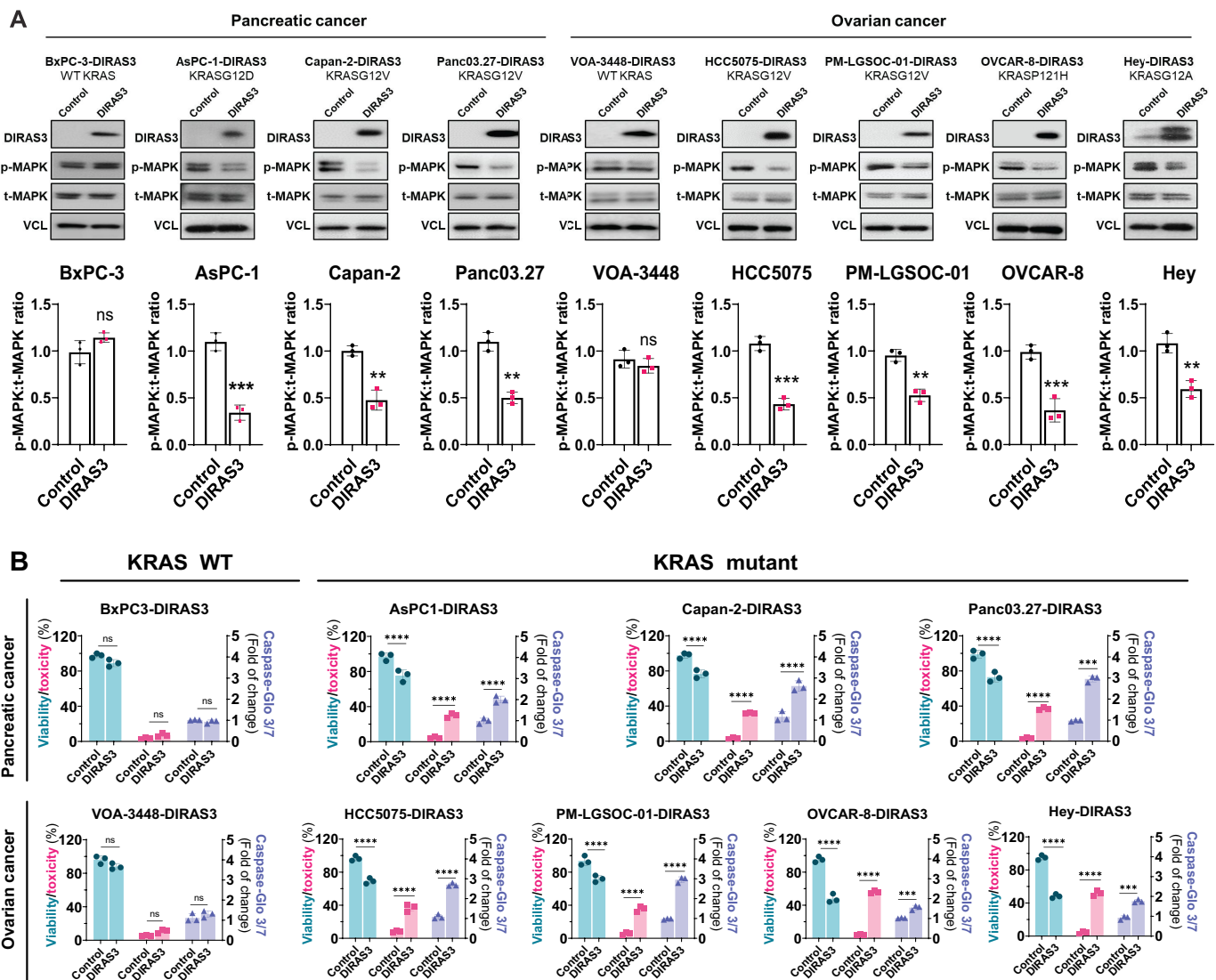


Figure 1. Induction of DIRAS3 expression inhibits KRAS-MAPK signaling and KRAS-driven tumor growth in KRAS mutant pancreatic and ovarian cancer cells. (A) quantification of KRAS signaling with and without DIRAS3 expression. Cancer cells were seeded at $0.2\text{--}0.4 \times 10^6$ cells/well and treated with DOX (1 $\mu\text{g}/\text{ml}$) for 48–72 h. Signal density was measured with ImageJ (imagej.nih.gov/ij/docs/guide/). The ratio of p-MAPK/ERK to t-MAPK/ERK was calculated and normalized to the DOX⁻ control. Statistical testing was performed by a two-sided t-test. (B) determination of DIRAS3's effect on cell viability, toxicity, and apoptosis. Cells were seeded at 5×10^3 cells/well in triplicate in a 96-well plate with or without DOX (1 $\mu\text{g}/\text{ml}$) for 72 h. Cell viability, cell toxicity, and apoptosis were assessed with CellTiter-glo, CellTox Green (left Y-axis), and caspase-glo 3/7 (right Y-axis) assays, respectively. All experiments were performed at least three times with similar results. Statistical testing was performed by two-way ANOVA. The columns indicate the mean and the bars indicate the SD (ns: $p > 0.05$, ** $p < 0.01$, *** $p < 0.001$, **** $p < 0.0001$).

mutationally activated BRAF rather than mutant KRAS, showed no change in p-MAPK/ERK upon DIRAS3 expression, further supporting that DIRAS3 decreased p-MAPK/ERK by blocking KRAS function, but not directly inhibiting BRAF activity. Next, we measured cell growth, cytotoxicity, and apoptosis in PDAC and ovarian cancer cell lines with and without DIRAS3 expression. Expression of DIRAS3 inhibited tumor cell growth and induced apoptosis in PDAC and ovarian cancer harboring mutant KRAS, but not in PDAC and ovarian cancer with WT KRAS (Figure 1B). Together these data support the conclusion that DIRAS3 preferentially blocks mutant KRAS signaling and induces cytotoxicity/apoptosis in PDAC and ovarian cancer with mutant KRAS.

DIRAS3 expression increases ROS-mediated cytotoxicity in PDAC and ovarian cancer cell lines driven by different KRAS mutations, but not in PDAC and ovarian cancer cell lines with WT KRAS

Mutant KRAS increases the transcription of NFE2L2, which stably elevates the basal NFE2L2 antioxidant program, and lowers intracellular ROS, permitting cancer cell survival [11,12]. We hypothesized that DIRAS3 expression increases the accumulation of ROS and induces cytotoxicity by blocking KRAS signaling while downregulating antioxidant activity. We measured ROS production in the presence and absence of DIRAS3 induction and found that DIRAS3 expression elevated ROS accumulation in KRAS mutant PDAC and LGSOC cell lines, but not in cancer cells with WT KRAS (Figure 2A). To test whether DIRAS3-induced ROS accumulation produced the cytotoxicity and apoptosis observed, we neutralized ROS by treating cancer cells with N-acetyl cysteine (NAC), an ROS scavenger. We found that DIRAS3 expression significantly increased ROS production and apoptosis (Figure 2B). When cancer cells were treated with NAC, levels of ROS and cytotoxicity/apoptosis were both substantially reduced (Figure 2C), suggesting that DIRAS3 inhibition of KRAS-induced cell death in mutant KRAS cancer cells is ROS-dependent. To determine the underlying mechanisms of DIRAS3-induced increases in ROS levels, we examined whether DIRAS3 regulates the transcription factor NFE2L2, which controls a panel of antioxidant genes, and we also evaluated MYC and JUN, upstream regulators of NFE2L2 that are induced downstream of KRAS signaling. We found that DIRAS3 expression significantly downregulated the mRNA expression of MYC and JUN, as well as their downstream target NFE2L2 (Figure 2D), suggesting that DIRAS3 transcriptionally regulates NFE2L2 through inhibiting mutant KRAS signaling. Moreover, we evaluated NFE2L2 protein levels in nuclear and cytoplasmic fractions and the expression of a panel of antioxidant genes regulated by NFE2L2 and found that DIRAS3 expression resulted in an approximately two-fold decrease of NFE2L2 protein levels in both cytoplasmic and nuclear fractions compared to control cells without DIRAS3 expression (Figure 2E). The mRNA expression of NFE2L2 target genes was significantly decreased, consistent with the downregulation of NFE2L2 (Figure S1). Depletion of NFE2L2 by siRNA substantially blocked DIRAS3-

induced ROS and cytotoxicity in mutant PDAC and LGSOC cells (Figure 2F). These data suggest that oncogenic mutant KRAS promotes tumor cell survival by activating defense mechanism(s) against oxidative stress. DIRAS3 expression disrupts the redox-antioxidant balance and induces ROS-mediated apoptosis by inhibiting mutant KRAS function and impairing the activation of the NFE2L2 transcriptional program (Figure 2G).

DIRAS3 expression inhibits mutant KRAS signaling, activates the energy-sensing STK11/LKB1-AMPK cascade, and induces autophagic flux

Despite the critical role of the RAS-MAP2K/MEK-MAPK/ERK signaling pathway in PDAC, MAP2K1/MEK1-MAP2K2/MEK2 inhibitors have failed to display clinical benefit in PDAC patients. DIRAS3 expression alone showed only modest cytotoxicity in PDAC and LGSOC by inhibiting RAS-MAP2K/MEK-MAPK/ERK signaling. As autophagy can act as a protective mechanism, we tested whether DIRAS3 could enhance the KRAS inhibition-induced STK11-AMPK energy-sensing cascade and induce autophagic flux. We examined DIRAS3-inducible cells in the presence and absence of DIRAS3 expression and observed that DIRAS3 expression decreased p-MAPK/ERK (Thr202/Tyr204) and p-STK11 (Ser428) and increased p-PRKAA (Thr172) in a time-dependent manner (Figure 3A). Moreover, the induction of autophagic flux by DIRAS3 is comparable to what was observed during nutrient deprivation, as shown by the decreased formation of autophagosomes (yellow) and increased formation of autolysosomes (red) in KRAS mutant PDAC and LGSOC cells stably expressing the mCherry-GFP-LC3 autophagy reporter (Figure 3B and S2A-C).

To confirm the ability of STK11 inhibition to abolish DIRAS3-induced autophagy in PDAC and LGSOC, we examined the conversion of endogenous LC3B-I to the lipidated, autophagosome-associated form, LC3B-II. We observed that both DIRAS3 expression and nutrient deprivation increased the conversion of LC3B-I to LC3B-II (increased the ratio of LC3B-II:LC3B-I) in cells treated with control siRNA, whereas treatment with siSTK11 decreased the conversion of LC3B-I to LC3B-II (resulting in a decrease in the ratio of LC3B-II:LC3B-I) after induction of autophagy by DIRAS3 or nutrient deprivation (Figure 4A). In a complementary approach, we showed that DIRAS3 expression significantly increased autophagic flux, as indicated by an increase in red fluorescent dots in cancer cells treated with control siRNA. However, DIRAS3-induced autophagic flux was abolished, as indicated by the presence of yellow fluorescent dots in cancer cells treated with siSTK11 (Figure 4B-C). Similar to the role of STK11, DIRAS3-mediated autophagy was also prevented when its downstream effector AMPK was inhibited by the simultaneous knockdown of PRKAA1 and PRKAA2 (Figure 4A-C). These results suggest that STK11-AMPK signaling is required for DIRAS3-induced autophagy in PDAC and LGSOC with mutant KRAS.

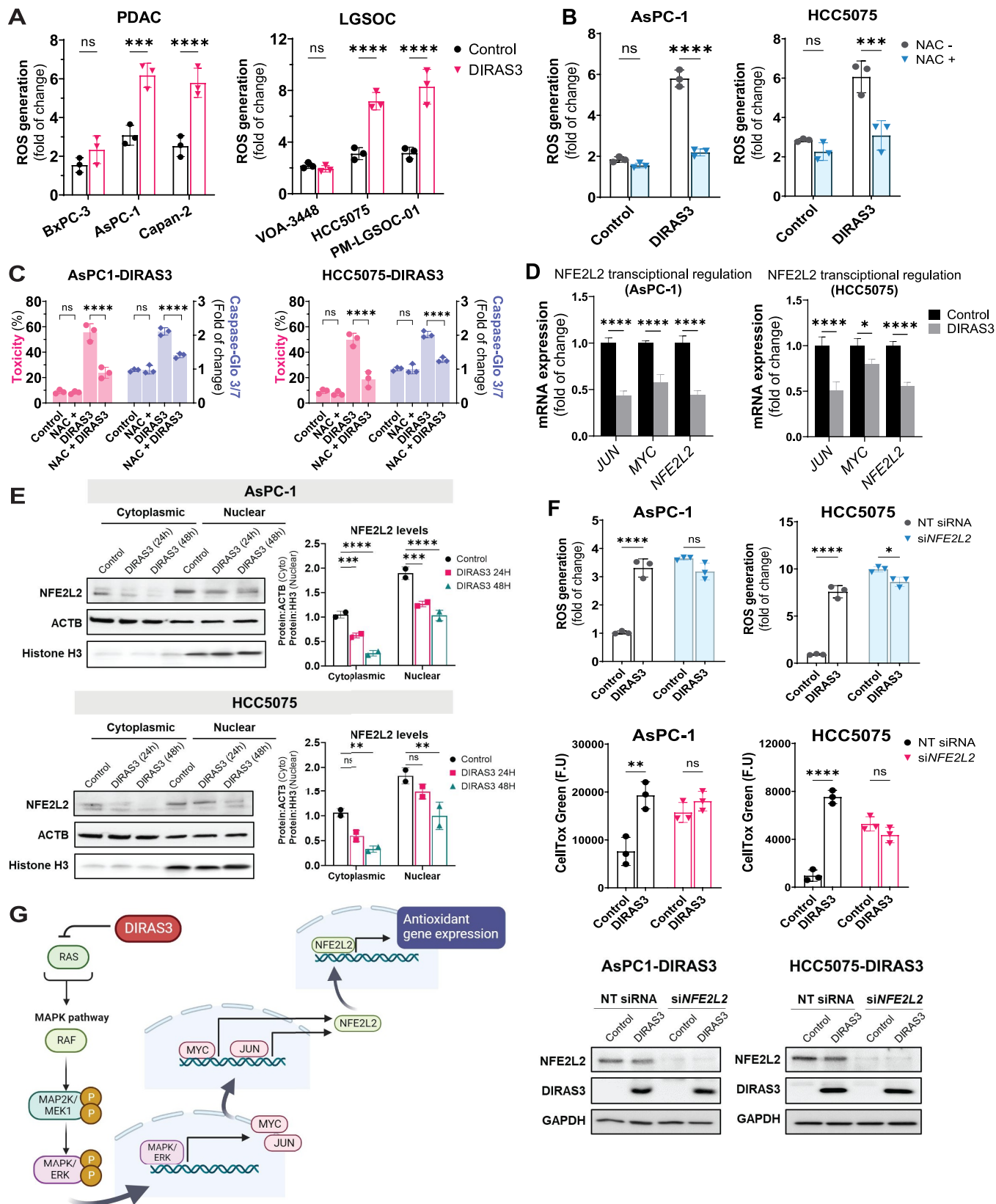


Figure 2. DIRAS3 increases ROS-mediated cytotoxicity by impairing the activation of the NFE2L2 transcriptional program in pancreatic and ovarian cancer cells driven by RAS mutations, but not in pancreatic and ovarian cancer cells with WT KRAS. (A and B) evaluation of ROS production. Cells were seeded at 5×10^3 cells/well in triplicate in 96-well plates with or without DOX (1 μ g/ml) for 72 h and a luminescence signal of ROS production was measured after 45 min incubation with DCFDA (20 μ M). For ROS scavenger experiments, 10 mM of NAC was added to culture media 24 h before ROS measurement. (C) analysis of cytotoxicity and apoptosis with and without NAC treatment. Cells were seeded at 5×10^3 cells/well in triplicate in 96-well plates with or without DOX (1 μ g/ml) and NAC (10 mM) was added to culture media 24 h before ROS measurement. Cytotoxicity and apoptosis were assessed with CellTox Green (left Y-axis) and caspase-glo 3/7 (right Y-axis) assays,

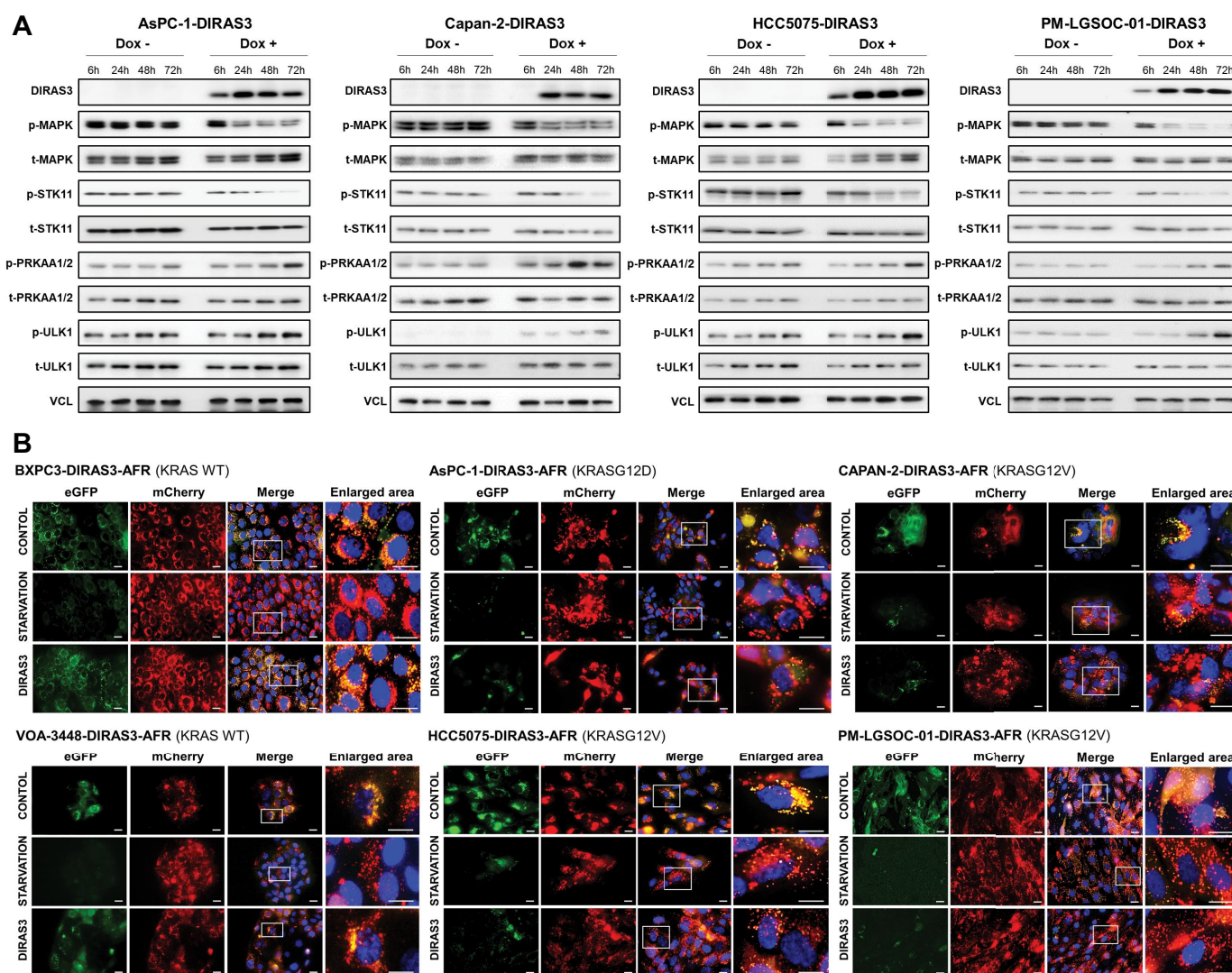


Figure 3. Inhibition of the RAS-MAP2K/MEK-MAPK/ERK signaling pathway induces autophagic flux by the stress-activated STK11-AMPK-ULK1 signaling axis in KRAS-driven pancreatic and ovarian cancer cells. (A) assessment of KRAS and STK11-AMPK signaling. Cells were seeded at 0.2×10^6 cells/well and treated with DOX (1 $\mu\text{g}/\text{ml}$) for 6 h to 72 h before cell lysates were collected. (B) analysis of autophagic flux by mCherry-eGFP-tagged-LC3B cells. An increased mCherry:eGFP ratio represents increased autophagic flux. Cells were treated with DOX for 48 h or 4 h in EBSS medium. Representative images are presented here, and image quantifications from the analysis of 5 separate high-power field images are listed in figure S2. All experiments were repeated three times with similar results. (scale bar: 10 μm).

DIRAS3-mediated activation of the STK11-AMPK pathway leads to CDKN1B-mediated autophagy in the cytoplasm

AMPK sensing of reduced cellular energy levels can activate ULK1 kinase. When cells are deprived of nutrients, activation of AMPK inhibits MTORC1, leading to ULK1-AMPK interaction and eventually the initiation and induction of autophagy. However, cytoplasmic CDKN1B also controls Ragulator and MTOR activity in nutrient-deprived cells to regulate the autophagy-lysosomal pathway [13]. Having shown that the STK11-AMPK pathway is triggered and activated after

DIRAS3-mediated KRAS inhibition and depletion of ULK1/ULK2 did not block DIRAS3-induced autophagy (Figure S3A-C), we investigated the energy-sensing pathway that regulates autophagy in KRAS mutant-driven PDAC and LGSOC by examining the role of CDKN1B. Threonine 198 phosphorylation (Thr198) of CDKN1B, regulated by the STK11-AMPK pathway, stabilizes CDKN1B localization in the cytoplasm [14]. DIRAS3 expression increased the retention of CDKN1B in the cytoplasmic fraction, while its levels were decreased in the nuclear fraction in two PDAC and two

respectively. (D) assessment of mRNA expression of JUN, MYC, and NFE2L2. Cells were seeded at 0.5×10^6 cells/well in 6-well plates with or without DOX (1 $\mu\text{g}/\text{ml}$) for 48 h before RNA isolation. (E) analysis of NFE2L2 protein levels in both nuclear and cytoplasmic fractions. Cells were seeded at 1×10^6 cells/100 mm dish and treated with DOX (1 $\mu\text{g}/\text{ml}$) for 48 h. Cell lysates were collected and fractionated. (b) detection of ROS and cytotoxicity with and without siNFE2L2. Cells were transfected with 25 nM of either control siRNA or siNFE2L2 (pool siRNA). DOX (1 $\mu\text{g}/\text{ml}$) was added 24 h post-transfection. ROS generation and cell viability were analyzed 72 h post-transfection. All experiments were performed at least three times with similar results. Statistical testing was performed by two-way ANOVA. The columns indicate the mean and the bars indicate the SD (ns: $p > 0.05$, ** $p < 0.01$, *** $p < 0.001$, **** $p < 0.0001$).

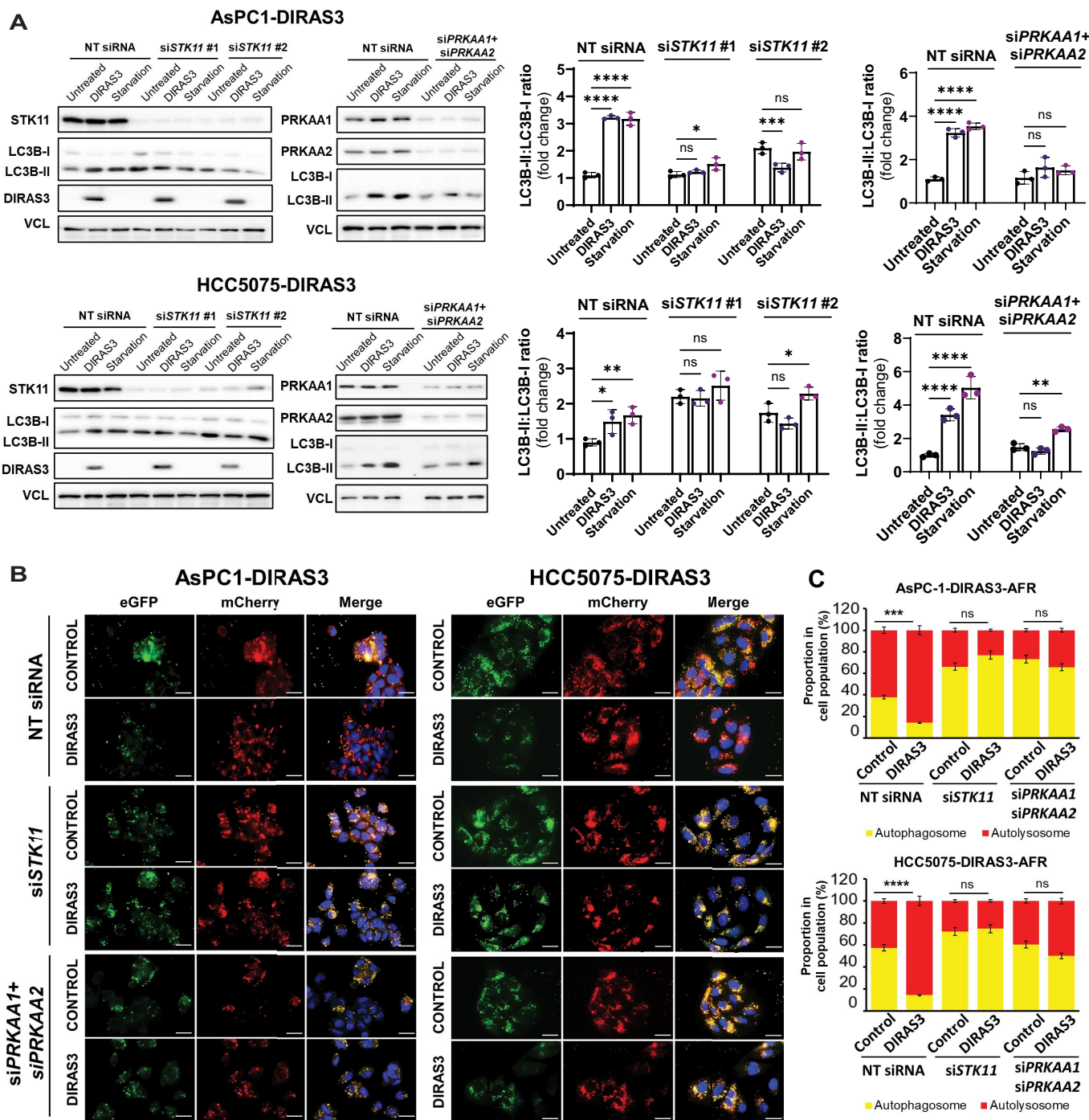


Figure 4. STK11-AMPK signaling is required for DIRAS3-mediated autophagy in PDAC and LGSOC with mutant KRAS. (A) assessment of autophagy with and without knockdowns of STK11 or PRKAA1 and PRKAA2. Cells were transfected with siControl, siSTK11, or siPRKAA1+siPRKAA2 (25 nM). DOX (1 μ g/ml) was added 24 h post-transfection. The ratio of LC3B-II:LC3B-I was calculated and indicated as a fold change by comparison to the first sample of each blot panel. Statistical testing was performed by two-way ANOVA. The columns indicate the mean and the bars indicate the SD (ns: $p > 0.05$, * $p < 0.05$, ** $p < 0.01$, *** $p < 0.001$, **** $p < 0.0001$). (B and C) measurement of autophagic flux with and without siSTK11 or siPRKAA1+siPRKAA2. Representative images and signal quantifications are presented from the analysis of 5 separate high-power field images (scale bar: 10 μ m). Experiments were repeated three times with similar results. Statistical analysis was performed with a two-sided t-test of control versus experimental groups; ns: $p > 0.05$, *** $p < 0.001$, **** $p < 0.0001$. Error bars represent SD.

LGSOC cell lines (Figure 5A). Co-localization of CDKN1B with the lysosomal marker LAMP1 was significantly higher in DIRAS3-induced cells compared to control cells (Figure 5B), suggesting that lysosomal localization of CDKN1B may be important for DIRAS3-induced autophagy in PDAC and LGSOC driven by mutant KRAS. Knockdown of *CDKN1B* with siRNA dramatically blocked the conversion of LC3B-I

to LC3B-II and prevented DIRAS3-mediated- and starvation-induced autophagy (Figure 5C). While induction of DIRAS3 enhanced autophagic flux in control cells, as shown by an increased mCherry/eGFP ratio, DIRAS3 failed to induce autophagic flux in CDKN1B knockdown cells (Figure 5D,E). In addition, to determine whether CDKN1B's induction of autophagy is related to its inhibition of CDK2 and CDK4 in cell

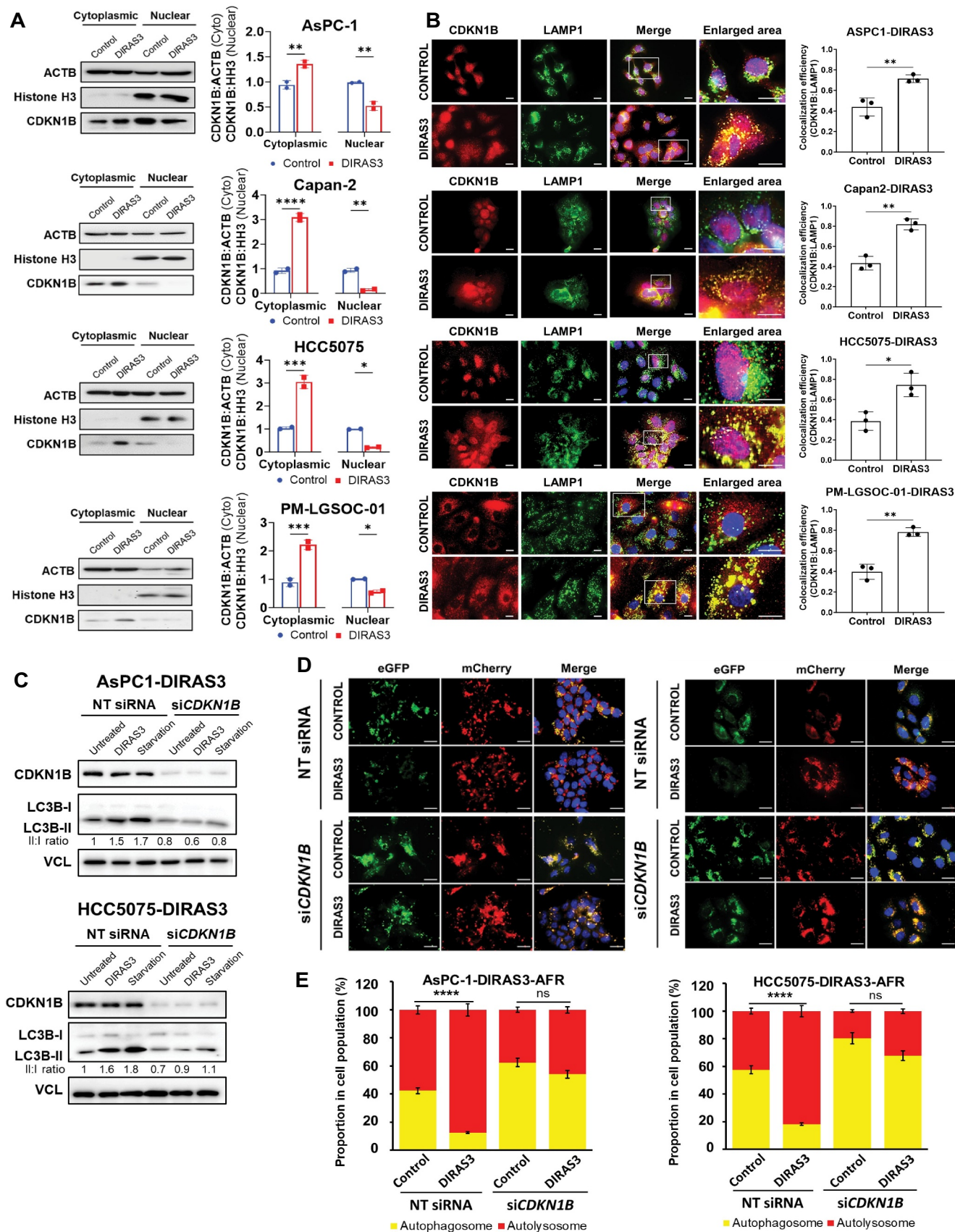


Figure 5. Cytoplasmic localization of CDKN1B is a key mediator of DIRAS3-mediated autophagy in PDAC and LGSOC cells. (A) evaluation of CDKN1B protein levels in both nuclear and cytoplasmic fractions. Cells were seeded at 1×10^6 cells/100 mm dish and treated with DOX (1 μ g/ml) for 48 h. Cell lysates were fractionated. Cytoplasmic and nuclear ratios of CDKN1B were normalized to beta-actin and histone H3, respectively. Statistical testing was performed by two-way ANOVA. The columns indicate the mean and the bars indicate the SD (ns: $p > 0.05$, ** $p < 0.01$, *** $p < 0.001$, **** $p < 0.0001$). (B) analysis of CDKN1B and LAMP1 colocalization. Images were captured on Olympus 1×71 Fluorescence Microscope and colocalization efficiencies were calculated using ImageJ, from the

cycle regulation, we treated cancer cells with either DOX or with starvation media, in the presence or absence of control siRNA or CDK2/CDK4 siRNA. Despite the downregulation of CDK2 and CDK4, DIRAS3 expression was still able to induce autophagy, as indicated by the increase in LC3B-I:LC3B-II conversion (increased the ratio of LC3B-II:LC3B-I) and decrease in SQSTM1 levels (Figure S4A). Therefore, cytoplasmic CDKN1B appears to be a critical regulator of stress-mediated autophagy triggered by the inhibition of oncogenic mutant KRAS, and its effects on autophagy seem to be independent of cell cycle regulation.

DIRAS3 induces CDKN1B-mediated nuclear localization of the transcription factor EB (TFEB), enhancing the expression of autophagy-related genes

Since CDKN1B prevents Ragulator and MTOR recruitment to lysosomes by disrupting Ragulator function [13] and DIRAS3 expression increased CDKN1B lysosomal localization, we hypothesized that DIRAS3 expression would decrease MTOR activity and increase transcriptional activity of TFEB and MITF, “master regulators” of autophagy and lysosome biogenesis [15,16]. To test this hypothesis, first, we analyzed the MTOR activity and localization over time after the expression of DIRAS3. DIRAS3 reduced phosphorylation of MTOR in a time-dependent manner, with the most prominent reduction starting around 48 h (Figure S4B). These results were supported by immunofluorescent staining showing decreased MTOR localization on the lysosomes in both pancreatic and low-grade ovarian cancer cells (Figure S4C). To further evaluate TFEB and MITF transcriptional program, we compared the nuclear localization of TFEB in control cells to that in DIRAS3-induced cells in four different cell lines (Figure 6A and S5A). DIRAS3 expression significantly enhanced the nuclear localization of TFEB in all four cell lines (Figure 6A and S5A). We also found that DIRAS3 expression promoted the nuclear translocation of both TFEB and MITF compared to the control, although the cytoplasmic levels of TFEB and MITF were either slightly decreased or unchanged by DIRAS3 expression (Figure 6B and S5B). To further confirm that CDKN1B regulates TFEB and that DIRAS3-mediated CDKN1B activation promotes nuclear localization of TFEB and increases the expression of downstream targets that regulate autophagy and lysosomal biogenesis, we transfected CDKN1B with siRNA in cells with and without DIRAS3 expression. DIRAS3 expression failed to promote TFEB localization (Figure 6C) or to increase the expression of TFEB target genes after the knockdown of CDKN1B (Figure 6D). By contrast, DIRAS3 expression significantly

increased the nuclear localization of TFEB (Figure 6C) and the expression of autophagy and lysosomal genes (Figure 6D) in the control siRNA group. Thus, DIRAS3 appears to activate autophagy through CDKN1B-mediated activation of transcription factors MITF/TFE in PDAC and LGSOC with mutant KRAS.

DIRAS3-induced autophagy protects KRAS mutant cancer cells from apoptosis

To determine whether DIRAS3-induced autophagy plays a role in protecting cancer cells from oxidative stress and cell death, we evaluated autophagic flux, cell viability, and apoptosis by knocking down the two critical genes *ATG5/Atg5* and *ATG7/Atg7* that are required for autophagosome formation. Treatment with si*ATG5/Atg5* and si*ATG7/Atg7* decreased cell viability (Figure 7A and S6A) and increased apoptosis (Figure 7B) compared to treatment with siControl in all the lines we examined, regardless of the KRAS mutation status. In contrast to siControl, si*ATG5/Atg5* or si*ATG7/Atg7* further reduced cell viability (Figure 7A) and increased apoptosis (Figure 7B) in KRAS mutant cancer cells when DIRAS3 was expressed, but si*ATG5/Atg5* or si*ATG7/Atg7* did not further reduce cell viability and apoptosis in WT KRAS cells, even though si*ATG5/Atg5* or si*ATG7/Atg7* blocked the induction of autophagy, as indicated by the decrease in the conversion of LC3B-I to LC3B-II in both mutant and WT KRAS cells (Figure 7A,B and S6A). These results suggest that DIRAS3-induced autophagy protects KRAS mutant cancer cells from cytotoxicity and apoptosis.

Chloroquine (CQ) and DC661 inhibit autophagy and enhance DIRAS3-induced cytotoxicity by increasing ROS production

As DIRAS3 induced protective autophagy in PDAC and LGSOC, we treated PDAC and LGSOC cells with CQ and DC661 and found that both significantly inhibited basal autophagy and decreased cell viability in a dose-dependent manner in all four cell lines regardless of KRAS status (Figure S6B-C). Then, we calculated the IC₅₀ of CQ and DC661 in PDAC and LGSOC cell lines to determine whether CQ and DC661 block DIRAS3-induced autophagy and enhance DIRAS3-induced cytotoxicity. We found that both CQ or DC661 in the presence of DIRAS3 further increased the sensitivity of all four mutant KRAS cell lines (up to 2.5 fold for CQ and up to 2 fold for DC661), but had minimal effects on KRAS WT BxPC-3 (1.1 for CQ and 0.96 for DC661) and VOA-3448 cells (1.05 for CQ and 1.17 for DC661) (Figure S6D). Noticeably, the IC₅₀ of CQ or DC661 was relatively lower across mutant KRAS PDAC and LGSOC cell lines when

analysis of 5 separate high-power field images (scale bar: 10 μ m). Statistical analysis was performed with a two-sided t-test (ns: $p > 0.05$, * $p < 0.05$, ** $p < 0.01$). Error bars represent SD. (C) evaluation of autophagy marker with and without si*CDKN1B*. Cells were transfected with 25 nM of either control siRNA or si*CDKN1B* (pool siRNA) and added with or without DOX 24 h after siRNA transfection. The ratio of LC3B-II:LC3B-I was calculated and indicated as a fold change by comparing it to the first sample of each gel panel. (D and E) assessment of autophagic flux with and without si*CDKN1B*. Representative images and the mCherry:eGFP ratios from the analysis of 5 separate high-power field images were calculated using ImageJ (scale bar: 10 μ m). Statistical analysis was performed with a two-sided t-test ns: $p > 0.05$, **** $p < 0.0001$. Error bars represent SD. All experiments were repeated three times with similar results.

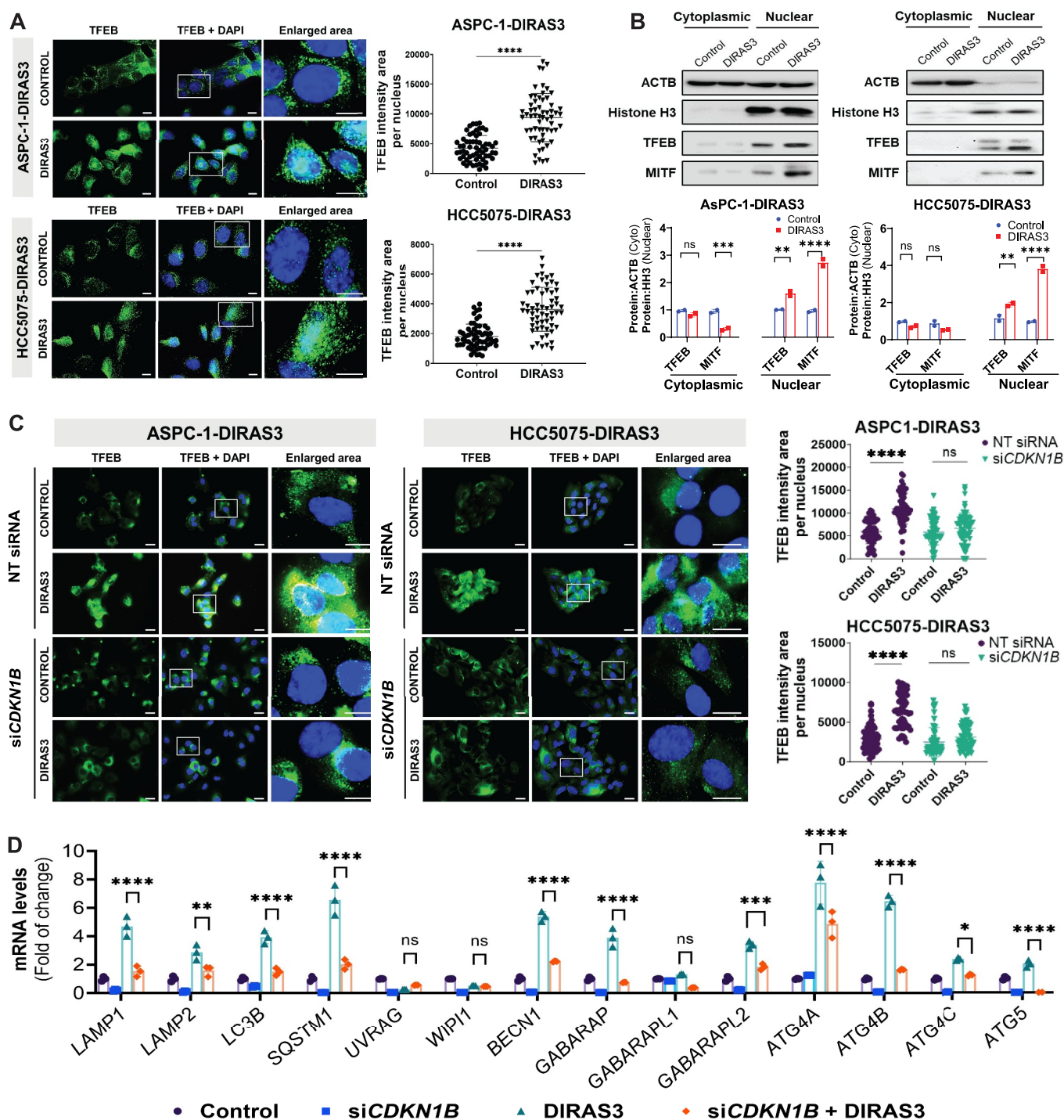


Figure 6. DIRAS3 induces CDKN1B-mediated nuclear localization of the TFEB transcription factor and enhances the expression of autophagy-related genes. (A) assessment of TFEB nuclear localization. Cells were treated with DOX (1 μ g/ml) for 48 h. TFEB intensity per nucleus was calculated by analyzing 60 nuclei per group with ImageJ (scale bar: 10 μ m). Statistical analysis was performed with a two-sided t-test. (**** p < 0.0001). Error bars represent SD. (B) analysis of TFEB and MITF nuclear and cytoplasmic fractions. Cells were treated with DOX for 48 h. Cytoplasmic and nuclear ratios of TFEB and MITF were normalized to beta-actin and histone H3, respectively. Statistical testing was performed by two-way ANOVA. The columns indicate the mean, and the bars indicate the SD (ns: p > 0.05, ** p < 0.01, *** p < 0.001, **** p < 0.0001). (C) quantification of nuclear localization of TFEB with and without siCDKN1B. Cells were transfected with 25 nM of either control siRNA or siCDKN1B. DOX (1 μ g/ml) was added 24 h post-transfection. TFEB intensity per nucleus was calculated by analyzing 60 nuclei per group with ImageJ (scale bar: 10 μ m). Statistical analysis was performed with a two-sided t-test. (D) quantification analysis of TFEB target genes. Cells were treated with siRNA and with or without DOX for 48 h. qPCR was performed to analyze TFEB target genes. All experiments were performed at least three times. The columns indicate the mean and the bars indicate the SD (ns: p > 0.05, ** p < 0.01, *** p < 0.001, **** p < 0.0001).

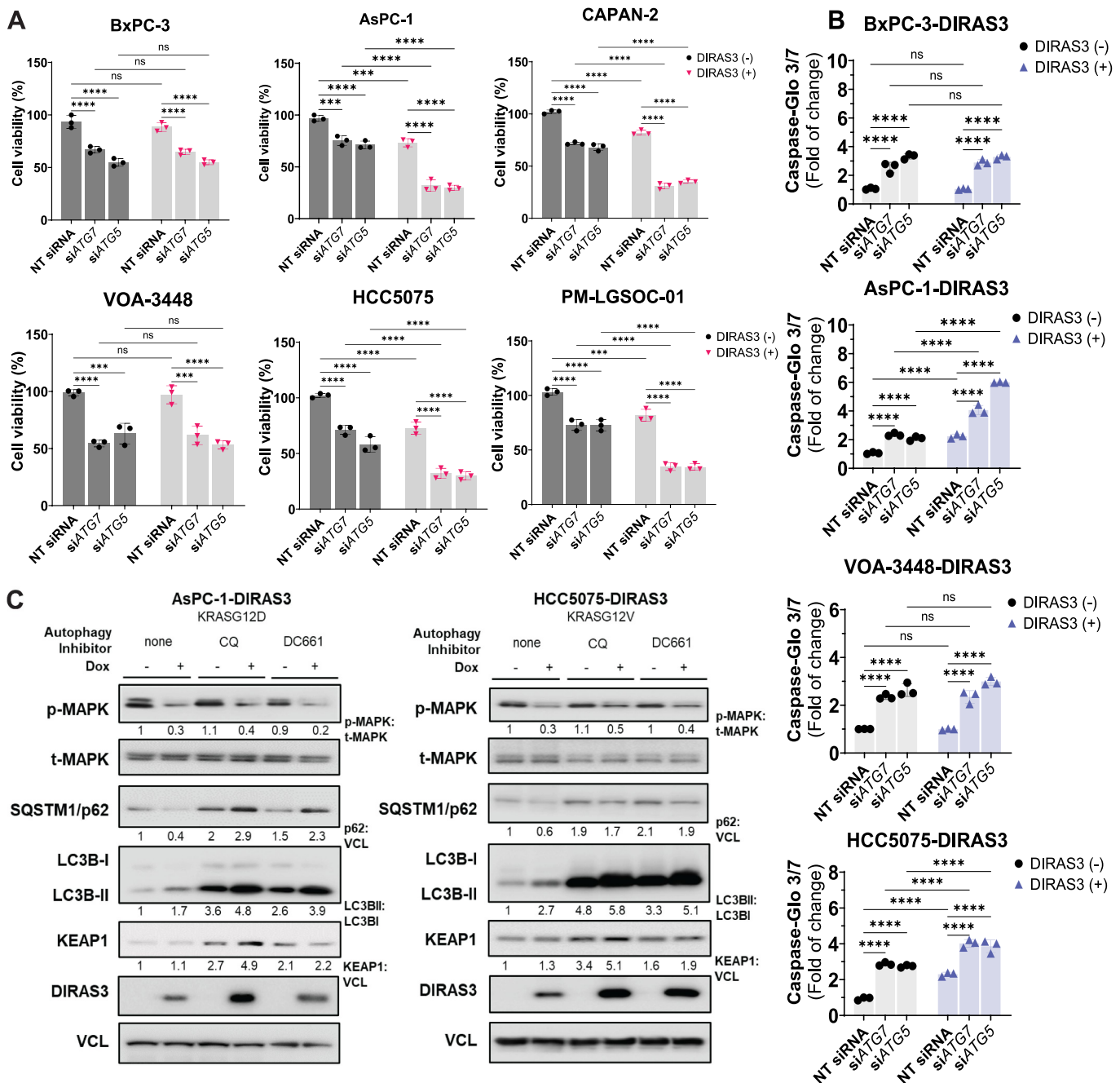


Figure 7. DIRAS3-mediated KRAS inhibition induces cytoprotective autophagy and enhances sensitivity to autophagy inhibition therapy in KRAS-driven PDAC and LGSOC in vitro. Evaluation of cell viability (A) and apoptosis (B) with and without siATG5 and siATG7. Cells were treated with siRNA for 24 h and then incubated with or without DOX for an additional 48 h. Experiments were repeated three times with three replicates for each experiment. Statistical testing was performed with two-way ANOVA (ns: $p > 0.05$, *** $p < 0.001$, **** $p < 0.0001$). Error bars represent SD. (C) assessment of KEAP1 expression with and without CQ or DC661. cells were seeded at 0.2×10^6 cells/well and treated with CQ (20 μ M) or DC661 (1.5 μ M) in the presence or absence of DOX (1 μ g/ml) for 48 h. Experiments were performed at least three times. The ratios of p-MAPK to t-MAPK, LC3B-II to LC3B-I, and SQSTM1/p62 to VCL were calculated and normalized to the control. Experiments were repeated three times with similar results.

DIRAS3 was expressed, compared to the IC₅₀ levels observed in BxPC-3 and VOA-3448 cells, suggesting that DIRAS3 increases the vulnerability of mutant KRAS PDAC and LGSOC cells to autophagy inhibitors. Although DC661 had a similar effect as CQ, it appeared to be more potent, with an IC₅₀ that was much lower than CQ in all the cell lines examined (Figure S6D). Finally, we evaluated ROS production and

showed that treatment with CQ and DC661 significantly increased ROS production and apoptosis compared to control in all six cell lines regardless of KRAS status (Figure S6E). However, CQ or DC661 enhancement of DIRAS3-mediated ROS levels and apoptosis was only observed in mutant KRAS cancer cells, not in cancer cells with WT KRAS (Figure S6E). As the transcription factor NFE2L2 regulates the expression of

several ROS detoxifying genes and SQSTM1/p62 activates NFE2L2 by interacting with and degrading the NFE2L2 inhibitor KEAP1 via autophagosomal degradation [17,18], we examined the expression of p-MAPK/ERK, SQSTM1/p62, LC3-I/II, and KEAP1. DIRAS3 induction decreased p-MAPK/ERK and SQSTM1/p62 and increased LC3B-I to LC3B-II conversion, indicating enhancement of autophagic flux in mutant KRAS cancer cells, but not in cancer cells with WT KRAS (Figure 7C and S6F). CQ or DC661 treatment significantly blocked autophagic flux, as indicated by increased levels of LC3BI and SQSTM1/p62, although it did not affect p-MAPK/ERK (Figure 7C and S6F). When autophagy was inhibited by CQ or DC661, preventing the degradation of SQSTM1/p62, led to the accumulation of KEAP1. Notably, the mutant KRAS cells expressing DIRAS3 exhibited greater accumulation of KEAP1 (Figure 7C). We further evaluated the effects of KEAP1 accumulation on NFE2L2 localization, we found that CQ and DC661, in turn, reduced NFE2L2 nuclear localization (Figure S7A) and down-regulated NFE2L2-regulated antioxidant gene expression (Figure S7B and C). Together, these results indicate that the autophagy inhibitors block DIRAS3-induced protective autophagy by disrupting the oxidant/antioxidant balance through the SQSTM1/p62-KEAP1-NFE2L2 pathway, preventing ROS clearance and enhancing cytotoxicity in mutant KRAS cancer cells.

Inhibition of autophagy significantly enhanced DIRAS3-induced inhibition of tumor growth in KRAS-driven PDAC xenograft models

To confirm that the findings in cell culture are relevant to tumor growth in vivo, we evaluated the effect of inhibiting KRAS with DIRAS3 expression and inhibiting autophagy individually and in combination in two xenograft models in athymic nu/nu mice. One week after cell injection, groups of mice were treated with vehicle control, DOX, CQ, DC661, or the combination of DOX+CQ or DOX+DC661 (Figure 8A). In both models, CQ and DOX as single agents had modest effects. However, DIRAS3 expression in the presence of CQ significantly blocked tumor growth in a much more effective manner (Figure 8A and S8A). While DC661 treatment appeared more effective in inhibiting tumor growth compared to CQ treatment, DIRAS3 expression did not further enhance the effect of DC661 treatment on tumor growth, compared to using DC661 alone (Figure 8A and S8A).

To validate the signaling changes resulting from various treatments in vivo, we collected and individually examined tumor xenografts through western blotting and IHC staining. Our findings confirmed the induction of DIRAS3 expression in all tumors treated with DOX (Figure 8B,C). Furthermore, significant changes, including a decrease in p-MAPK/ERK, an increase in cleaved CASP3 (caspase 3) and PARP, and a reduction in p-HH3 (Figure 8B–D) were observed. The accumulation of LC3B-II and SQSTM1/p62 was enhanced following the induction of DIRAS3 expression, and this elevation was further enhanced by the addition of CQ treatment (Figure 8B,C). Collectively, these results strongly suggest that our in vivo study aligns with the mechanisms that were identified in vitro.

Discussion

Our previous studies demonstrated that DIRAS3 can inhibit the growth of cancers driven by HRAS and KRAS [10]. In this report, we extended our observations to include cancers driven by multiple KRAS mutations in human PDAC and LGSOC cells. We found that DIRAS3 inhibits RAS/MAPK/MAPK/ERK signaling, increases the accumulation of ROS, and paradoxically promotes protective autophagy in PDAC and LGSOC cells harboring KRAS mutations, but not in PDAC and LGSOC cells with WT KRAS. Further, we demonstrated that DIRAS3 activates the energy-sensing STK11-AMPK pathway, inducing CDKN1B-mediated activation of the MiT/TFE transcriptional program, enhancing autophagic flux in mutant KRAS cancer cells. DIRAS3 is a RAS-related small GTPase tumor suppressor that is frequently downregulated in multiple cancer types. Through its direct binding to RAS and formation of heterodimers, DIRAS3 disrupts RAS nanoclustering, leading to the inhibition of mutant RAS signaling and suppression of tumor cell growth [10]. DIRAS3 expression induces ROS-mediated cytotoxicity and apoptosis in PDAC and LGSOC cells driven by different KRAS mutations, while not affecting cells with wild-type KRAS. This suggests that DIRAS3 plays a crucial role in regulating mutant RAS-driven oncogenesis. One possible explanation is that DIRAS3 selectively affects the active, GTP-bound form of KRAS and its downstream signaling, as we found that DIRAS3 expression inhibits p-MAPK/ERK in wild-type KRAS cancer cells treated with EGF growth factor (data not shown). Another potential explanation is that DIRAS3 may reside in the same microdomain as GTP-bound KRAS since GDP-bound KRAS and GTP-bound KRAS form nanoclusters in different locations on the plasma membrane [19,20]. By interacting with phosphatidyserine (PS) (data not shown), DIRAS3 could potentially disrupt mutant KRAS nanoclusters on the PS-containing plasma membrane, leading to the inhibition of mutant KRAS-mediated signaling. While our study primarily focused on the effect of DIRAS3 on KRAS, we have previously demonstrated that DIRAS3 can inhibit malignant transformation in murine fibroblasts induced by both KRAS and HRAS. Therefore, the findings of our current study might also apply to HRAS.

Recently, the role of STK11-AMPK in sensing different types of stress has pointed to a conditional oncogenic role for this pathway. Its ability to modulate cell metabolism and cellular processes including autophagy may confer a survival advantage under selective pressure by favoring adaptation to hostile conditions [21]. Autophagy is a catabolic process by which intracellular components are captured, degraded, and recycled in membrane-bound lysosomal vesicles to sustain metabolism in nutrient-poor environments [22]. In RAS-driven cancer cells, autophagy is strongly upregulated by cellular stress and nutrient deprivation and provides an important cell survival mechanism by facilitating the recycling of essential nutrients, preventing the accumulation of misfolded proteins and ROS, maintaining organelle function, and regulating intracellular signaling pathways [23,24]. Previous research suggested that AMPK plays a role in autophagy induction through its regulation of ULK1. However,

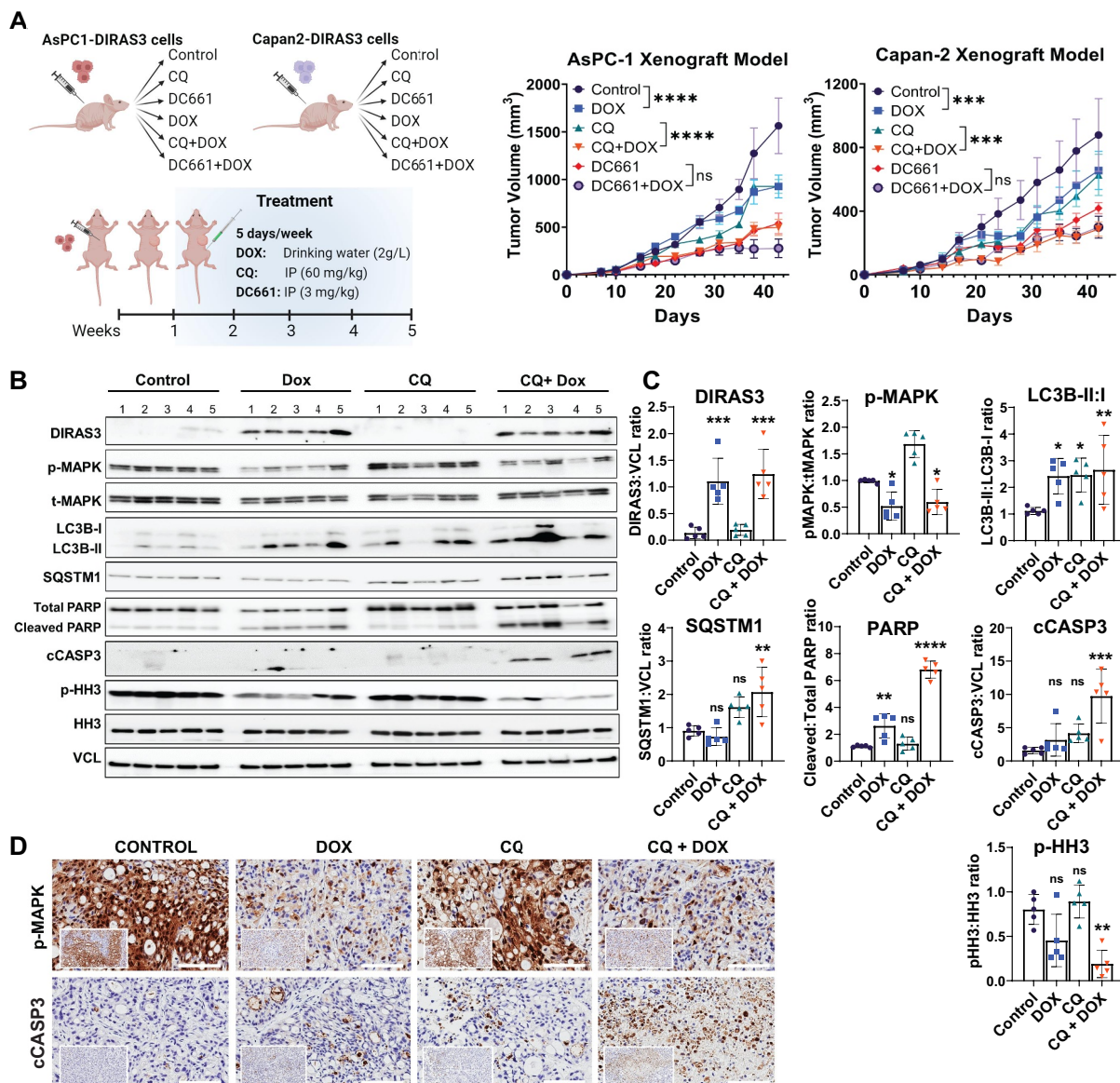


Figure 8. DIRAS3 enhances sensitivity to autophagy inhibition therapy in KRAS-driven PDAC xenograft models. (A) evaluation of DIRAS3, CQ, and DC661 function in PDAC xenograft models. The tumor growth curves were plotted with GraphPad. Statistical testing was performed with two-way ANOVA (ns: $p > 0.05$, *** $p < 0.001$, **** $p < 0.0001$). Error bars represent SD. (B) Western blot analysis of AsPC-1 xenograft tumors. Tumors were harvested from mice ($n = 5$) after 8 days of treatment, a total of 15 μg protein per sample was loaded. Individual antibodies were probed as indicated. (C) quantifications of the western blot signals were performed by ImageJ. Statistical testings were performed by one-way ANOVA. The columns indicate the mean and the bars indicate the SD (ns: $p > 0.05$, * $p < 0.05$, ** $p < 0.01$, *** $p < 0.001$, **** $p < 0.0001$). (D) immunohistochemical stainings for p-MAPK/ERK and cleaved CASP3 (cCASP3) in AsPC-1-DIRAS3 xenograft model (scale bar: 60 μm).

the cyclin-dependent kinase inhibitor CDKN1B is also a downstream target of the STK11-AMPK pathway, which senses cellular stress and energy levels. AMPK-dependent phosphorylation of CDKN1B at Thr198 stabilizes CDKN1B and allows cells to survive metabolic stress [14]. Importantly, cytoplasmic CDKN1B can also modulate MTOR signaling by inhibiting Ragulator assembly on the lysosomal membrane, activating the TFEB, a master regulator of autophagy and biogenesis, and thereby promoting autophagy during prolonged periods of stress [13]. We observed that depletion of CDKN1B significantly blocks DIRAS3-induced autophagic flux, while depletion of ULK1 and ULK2 did not have a similar effect, despite downregulating basal autophagy. This suggests that DIRAS3-mediated inhibition of mutant

KRAS selectively regulates phosphorylation of CDKN1B through the activation of the STK11-AMPK pathway, inhibition of MTOR, promoting TFEB nuclear localization and increasing the expression of key autophagy-related genes, leading to the induction of cytoprotective autophagy. Therefore, the inhibition of mutant KRAS by DIRAS3 triggers the transcriptional activation of the lysosomal-autophagy pathway as a response to cope with cellular stress in mutant KRAS PDAC and LGSOC.

ROS can promote antitumorigenic signaling and trigger oxidative stress-induced cancer cell death. To hyperactivate cell signaling pathways required for malignant transformation, cancer cells increase their rate of ROS production compared to normal cells. Concomitantly, in order to maintain

ROS homeostasis and evade cell death, cancer cells increase their antioxidant capacity [25]. We documented that DIRAS3-mediated inhibition of mutant KRAS promotes cancer cell death by disrupting the redox-antioxidant balance, impairing the activation of the NFE2L2 transcriptional program, and increasing ROS production. Paradoxically, DIRAS3-induced cytotoxicity was limited by DIRAS3-induced autophagy that promotes ROS degradation and protects cancer cells from ROS-mediated cytotoxicity. Compared to WT KRAS cancer cells, DIRAS3-induced autophagy might also increase the susceptibility of mutant KRAS cancer cells to inhibitors of autophagy. CQ is a clinically available antimalarial agent that also acts as an autophagy inhibitor [26]. DC661 is a novel dimeric CQ that can deacidify the lysosome and inhibit autophagy [27]. We demonstrated that CQ or DC661 significantly enhanced DIRAS3-induced cytotoxicity/apoptosis by disrupting the oxidant/antioxidant balance through the SQSTM1/p62-KEAP1 pathway and preventing ROS clearance in PDAC and LGSOC cells driven by mutant KRAS. This is a collective effect emerged by DIRAS3 expression and autophagy inhibition which involved a decrease in the nuclear localization of NFE2L2, leading to the down-regulation of antioxidant genes, and subsequently intensifying ROS-mediated cell death. Recently, we have found that stapled peptides derived from the $\alpha 5$ domain of DIRAS3 can significantly inhibit the growth of KRAS-driven PDAC cell lines and xenografts [28]. In future studies, inhibiting mutant KRAS with DIRAS3-derived peptides and autophagy inhibitors should be a promising strategy.

Overall, our study demonstrates that the expression of DIRAS3 preferentially blocks KRAS signaling in PDAC and LGSOC driven by different KRAS mutations, but not in PDAC and LGSOC with WT KRAS. Inhibition of mutant KRAS by DIRAS3 induces autophagy which promotes cancer cell survival. Thus, autophagy-mediated resistance to mutant KRAS inhibition can be overcome by treating cancer cells with autophagy inhibitors. While the current study focuses on PDAC and LGSOC, DIRAS3 is also downregulated in many other cancer types such as lung, breast, and colon cancers [29–32]. These findings offer potential insights into the underlying molecular mechanisms that drive the dependence on mutant KRAS in various types of cancer and may also guide the development of novel therapeutic strategies, such as the use of peptides derived from DIRAS3 in combination with autophagy inhibitors.

Materials and methods

Cell culture and maintenance

Pancreatic ductal adenocarcinoma cell lines were obtained from ATCC including AsPC-1 (KRAS^{G12D}; CRL-1682), BxPC-3 (KRAS WT, BRAF^{V600E}; CRL-1687), Capan-2 (KRAS^{G12V}; HTB-80), and Panc03.27 (KRAS^{G12V}; CRL-2549). The low-grade serous ovarian cancer cell line HCC5075 (KRAS^{G12V}) were obtained from Dr. Adi F. Gazdar, UT Southwestern Medical Center (Dallas, TX). VOA-3448 (KRAS WT) cells were obtained from Dr. Mark S. Carey, University of British Columbia (Vancouver, Canada) [33]. PM-LGSOC-01

(KRAS^{G12V}) cells were provided by Dr. Olivier De Wever, Ghent University (Ghent, Belgium) [34]. The OVCAR-8 (KRAS^{P121H}) and Hey (KRAS^{G12A}) ovarian cancer cells were provided by Dr. Gordon Mills, UT M.D. Anderson Cancer Center (Houston, TX). AsPC-1, Hey, BxPC-3, Panc03.27, OVCAR-8, and HCC5075 cells were routinely grown in RPMI-1640 (Corning, 15-040-CV) supplemented with 2 mM L-glutamine, and 10% fetal bovine serum (FBS), 100 U of penicillin and 100 μ g of streptomycin. Capan-2 cells were grown in McCoy's (Corning, 10-050-CV) supplemented with 10% FBS, 100 U of penicillin, and 100 μ g of streptomycin. PM-LGSOC-01 cells were grown in EMEM (Corning, 15-010-CV) supplemented with 10% FBS, 100 U of penicillin, and 100 μ g of streptomycin. VOA-3448 cells were grown in 1:1 mixture of M199 and MCDB media supplemented with 10% FBS, 100 U of penicillin, and 100 μ g of streptomycin. All cells were maintained in a humidified atmosphere of 5% CO₂ and 95% room air.

Generation of DIRAS3-inducible cell lines

To establish DIRAS3-inducible cell lines, cells were transfected with lentivirus carrying a DIRAS3 plasmid that was custom synthesized by Sirion Biotech to express DIRAS3 from a Tet-on inducible promoter. Cells were plated in a 6-well plate at ~70–80% confluence in antibiotic-free complete growth medium described above. The next day, the complete medium was replaced with antibiotic-free media supplemented with 8 ng/ml polybrene (Millipore Sigma, TR-1003-G), and cells were infected with lentivirus carrying the DIRAS3-encoding plasmid. At 18 h post-transduction, the virus-containing medium was replaced with complete growth media. At 48–72 h post-transduction, the cells then were placed in selection media that contained growth media supplemented with G418 (200–800 μ g/ml depending on cell line; Corning, 61-234-RG). DIRAS3 expression was induced by adding 1 μ g/ml doxycycline (DOX; Sigma-Aldrich, D9891) to the selection medium for 48 h and DIRAS3 levels were confirmed by western blot analysis. To eliminate heterogeneity in a mixed cell population containing various copy numbers of the *DIRAS3* gene and to obtain a homogenous population, single-cell clones were generated by serially diluting the DIRAS3-expressing pooled population. These clonal cell lines were then screened and those with the highest protein expression levels were expanded and used. All DIRAS3 inducible cell lines were maintained using tetracycline-free FBS and G418 (200–800 μ g/ml) to maintain clonal selection.

Generation of autophagic flux reporter (AFR) cell lines

DIRAS3-inducible pancreatic and ovarian cancer cells were infected with retrovirus carrying the pBabe-mCherry-eGFP-LC3 (C-G-LC3) plasmid (Addgene 22,418; deposited by Jayanta Debnath) to generate autophagic flux reporter cell lines. At 18 h post-transduction, the virus-containing medium was replaced with a complete growth medium. eGFP and mCherry expression was confirmed by fluorescence microscopy 48 h after transduction. Cells then were placed in selection media that contained growth media supplemented with

puromycin (1 µg/ml) and incubated for 48–72 h before sorting for mCherry and eGFP double-positive cells using narrow gates.

Flow cytometry

Following selection for the highest sensitivity and reproducibility, a heterogeneous population of transduced cells was sorted with flow cytometry for mCherry and GFP double-positive cells using small gates to obtain a high-expression and a medium-expression population. These sorted doubly positive pools were grown and cells were tested for their ability to measure autophagic flux. Then each population was expanded and autophagic flux was measured by immunofluorescence microscopy using the ratio of mCherry to eGFP [35]. The AFR cell lines were routinely grown in the same medium noted above supplemented with puromycin (0.5–1 mg/ml) to maintain clonal selection.

Generation of human PDAC xenografts in mice

DIRAS3-inducible and the parental AsPC-1 cells (1.2×10^6) and DIRAS3-inducible Capan-2 cells (3×10^6) were injected subcutaneously into eight-week-old female and male athymic nu/nu mice that were purchased from Envigo Biosciences. Each group contained 8–10 mice. Treatments started one week after the day of injection (initial tumor volumes were 46 ± 9.2 and 55.75 ± 12.3 for AsPC-1 and Capan-2 models, respectively). CQ (60 mg/kg; Sigma-Aldrich, C6628) and DC661 (3 mg/kg; TargetMol, T5538) were administered intraperitoneally 5 days/week for 4 weeks. Mice were given water with 2 mg/ml DOX in 5% sucrose (DIRAS3⁺ groups) or 5% sucrose alone (DIRAS3⁻ groups). Water was replaced every two days throughout the study. Tumors were measured twice a week; body weights were measured before and after treatment. When the tumor volume reached 2000 mm³ or a 5 mm ulcer was observed, mice were euthanized with CO₂. All procedures were carried out according to an animal protocol approved by the IACUC of The University of Texas MD Anderson Cancer Center.

Antibodies

Anti-DIRAS3 murine monoclonal antibodies (15E11 and 1D8) were developed in our laboratory. All other antibodies were obtained commercially: Antibodies against p-MAPK/ERK (Thr202/Tyr204; 4370S), t-MAPK/ERK (4695S), ACTB/ β -actin (4970), LC3B (3868), histone H3 (4499), STK11/LKB1 (3047), p-STK11/LKB1 (Ser428; 3482), PRKAA/AMPK α (5832), p-PRKAA/AMPK α (Thr172; 2535), ULK1 (8054), p-ULK1 (Ser555; 5869), MITF (12590), NFE2L2/Nrf2 (12721), KEAP1 (8047), CDK2 (18048), CDK4 (#12790), and GAPDH (2118) were purchased from Cell Signaling Technology. Anti-VCL/vinculin (V9264) and anti-p-MITF (Ser180/73; SAB4503940) were from Sigma. Antibodies against CDKN1B/p27 (sc-1641) were purchased from Santa Cruz Biotechnology; p-CDKN1B/p27/Kip1 (T198; AF3994) R&D Systems; TFEB (A303-673A) from Bethyl Laboratories; and SQSTM1/p62 (PM045) from MBL International.

siRNA transfections

siGENOME *STK11*, *PRKAA1*, *PRKAA2*, *ULK1*, *CDKN1B*, *CDK2*, and *CDK4* siRNAs and a control non-targeting siRNA pool were purchased from Horizon Discovery to generate knockdowns. siRNAs were initially resuspended in 1X siRNA Buffer (Horizon Discovery, B-002000-UB-100) at a stock concentration of 20 µM as described by Horizon Discovery's siRNA resuspension protocol. Then, 7.5 µl of this stock was added to 592.5 µl of room temperature OPTI-MEM media (Gibco 31,985,070), gently mixed, and added to the DharmaFECT (Horizon Discovery, T-2001-02):OPTI-MEM mixture (9 µl:591 µl). siRNA:DharmaFECT complex (400 ul per well) was added to triplicate wells in a 6-well plate and incubated at room temperature for 30 min. Cells were trypsinized and suspended at 1×10^6 cells/ml in an antibiotic-free complete media. Cells were added to each well containing siRNA:DharmaFECT complex to produce a final volume of 2 ml/well and incubated at 37°C in 5% CO₂ for 72 h. For experiments involving DIRAS3 re-expression, DOX (1 µg/ml) was added 24 h post-transfection. As a positive control for autophagy induction, cells were incubated in EBSS (Gibco 24,010,043) for 4 h to induce nutrient starvation-induced autophagy.

Immunoblotting

To prepare protein lysates, wells were washed twice with ice-cold PBS (Corning, 21-040-CV) and then cells were treated for 1 min at room temperature in 150 µl of SDS lysis buffer containing 62.5 mM Tris-HCl, pH 6.8, 2.5% SDS, 10% glycerol, 5% β -mercaptoethanol, and 0.002% bromophenol blue. Lysates were placed on a dry block at 99°C for 5 min. Subsequently, the whole cell lysates were separated by SDS-PAGE using 5–12% polyacrylamide and transferred to PVDF membranes. Immunoblot analysis was performed with the antibodies indicated and visualized with an ECL-enhanced chemiluminescence detection kit (SuperSignal™ West Pico PLUS; Thermo Scientific 34,580). Band intensity from western blots was quantified using the ImageJ program.

Immunocytochemistry

Immunofluorescence staining was performed using coverslips fixed with 4% paraformaldehyde at room temperature for 10 min before washing with PBS. Cells were permeabilized using 0.1% Triton X-100 (Sigma-Aldrich, T9284) in PBS for 10 min at room temperature. Cells were washed three times with 0.1% Tween 20 (MP Biomedicals, TWEEN201) in PBS (PBS-T) for 5 min each before being blocked with 3% BSA (Sigma-Aldrich, A9418) at room temperature for 1 h. Primary antibodies were added at a dilution of 1:50 in 3% BSA and incubated overnight at 4°C. Cells were washed three times with PBS-T for 5 min each before the addition of secondary antibodies. Secondary antibodies were added at a 1:200 dilution in 1.5% BSA and incubated at room temperature for 1 h. Cells were washed with PBS-T and stained with DAPI at a 1:10,000 dilution for 10 min at room temperature. Slides were mounted and images were captured on Olympus 1 × 71 Fluorescence Microscope.

Cell viability assay

Cells were seeded at 5×10^3 cells/well in black-wall 96-well plates and allowed to attach overnight at 37°C in 5% CO₂ and 95% humidified air. Control wells containing medium without cells were included to determine background luminescence. The treatments or transfections were performed the next day and cells were incubated for 72 h. The microplate was equilibrated to room temperature for 30 min prior to the addition of 100 μ l of CellTiter-Glo 2.0 (Promega, G9243) per well. The plate was shaken for two min to induce cell lysis and incubated at room temperature for 10 min to stabilize the luminescent signal before reading. The luminescence signal was recorded BioTek multi-plate reader.

Cytotoxicity assay

The cytotoxic effects of DIRAS3, autophagy inhibitors, and their combinations were assessed using CellTox Green Cytotoxicity Assays (Promega, G8743) according to the manufacturer's recommendations. Briefly, the cells were seeded into black wall 96-well plates (5×10^3 cells/well) in growth media. After 24 h, the growth media was replaced with fresh media containing serial concentrations of the compounds to be tested, and the cells were incubated for an additional 48 h. Then, freshly prepared CellTox Green Dye in assay buffer was added to wells, plates were shaken for 1 min at 750 rpm, and fluorescence signal (Ex: 485/Em: 520 nm) was measured in a BioTek multi-plate reader.

Apoptosis

The mechanisms of cell death induced by either DIRAS3, autophagy inhibitors, and their combinations were assessed using The Caspase-Glo[®] 3/7 assay (Promega, G8093) according to the manufacturer's recommendations. Cells were seeded into black wall 96-well plates (5×10^3 cells/well) in growth medium. The next day, the growth media was replaced with fresh medium containing serial concentrations of the compounds to be tested, and the cells were incubated for an additional 96 h. Then, freshly prepared Caspase-Glo[®] 3/7 Reagent was added to wells, and luminescence was recorded BioTek multi-plate reader. Background readings were determined from wells containing culture media without cells.

Measurement of ROS levels

Intracellular reactive oxygen species (ROS) activity was measured by reacting the cell-permeant fluorogenic reagent 2',7'-dichlorofluorescein diacetate (DCFDA, also known as H2DCFDA) (Abcam, ab113851) with living cells. The DCFDA assay is based on the diffusion of DCFDA dye into the cell followed by its deacetylation by cellular esterases to a non-fluorescent compound, which is later oxidized by ROS into 2', 7' -dichlorofluorescein. Cells were plated onto 96-well black-walled plates at a density of 5×10^3 cells/well. The next day, cells were treated based on the experimental groups

to be tested for 72 h. At the end of treatment, the cells were stained with 20 μ M DCFDA reagent, incubated for 45 min, washed with PBS, and analyzed by a BioTek multi-plate reader at Ex: 485 nm/Em: 535 nm.

Nuclear and cytoplasmic fractionation assay

Cells were seeded at 1×10^6 cells/100 mm dish and treated with DOX (1 μ g/ml) for 48 h. Cells were collected, and fractionated lysates were prepared with NE-PER Nuclear and Cytoplasmic Extraction Kits (ThermoFisher 78,833) using the manufacturer's recommended protocol. ACTB served as a control for cytoplasmic fractions while histone H3 was used for nuclear protein samples.

Immunohistochemical staining

Formalin-fixed and paraffin-embedded mouse tumor tissue sections were loaded onto the Leica Bond RX automated staining platform. The instrument executed an automated deparaffinization and rehydration protocol using BOND Dewax Solution (Leica, AR9222), 100% alcohol, and BOND Wash Solution (Leica, AR9590). Antigens were retrieved by BOND[™] Epitope Retrieval ER1 Solution (Leica, AR9961) at 100°C for 20 min. Tissues were blocked in Refine Detection Kit Peroxide Block (Leica, DS9800) for 5 min followed by 5% goat serum (Cell Signaling Technology, 5425) for 30 min. Primary antibody incubations were performed at room temperature, p-MAPK/ERK (Cell Signaling Technology, 4370) at 1:800 dilution for 45 min, and cleaved CASP3 (Biocare, CP229B) at 1:100 dilution for 60 min. Refine Detection Kit Polymer (Leica, DS9800) was applied for 8 min at room temperature followed by DAB chromogenesis with Refine Detection Kit Mixed DAB (Leica, DS9800). The automated platform executed washing steps using BOND Wash Solution. Counterstaining with hematoxylin was performed to enable nuclear visualization. Stained slides were examined under a light microscope, and digital images were captured using an attached camera. Positive control slides with known positive staining and negative control slides omitting the primary antibody were included to ensure proper staining quality and to evaluate nonspecific binding.

Gene expression analysis

AsPC-1-DIRAS3 and HCC5075-DIRAS3 cells were seeded into 6-well plates and treated with DOX (1 μ g/ml) for 24 and 48 h to induce DIRAS3 expression. RNA was isolated with Qiagen RNeasy Micro Kits (74004) and reverse transcribed to cDNA with SuperScript[™] First-Strand Synthesis System for RT-PCR (Thermo Scientific 11,904-018). 50 ng cDNA was used in a SYBR green-based quantitative PCR to measure mRNA expression. Relative expression was calculated by the 2- $\Delta\Delta$ CT method. GAPDH was used as a reference and shown as a fold of change. Primers included 5'→3'

Gene		Primer sequence (5'→3')
GAPDH	Forward	GAGTCAACGGATTTGGTCGT
	Reverse	TTGATTTTGGAGGGATCTCG
GPX2	Forward	AATTTGGACATCAGAAGTCTGC
	Reverse	GGCTGCTCTTCAAGATTTAG
JUN	Forward	AAAGGATAGTGCATGTTTC
	Reverse	TAAAATCTGCCACCAATTCC
MYC	Forward	TGAGGAGAAACAAGAAGATG
	Reverse	ATCCAGACTCTGACCTTTTG
NFE2L2	Forward	CGTTTGTAGATGACAATGAGG
	Reverse	AGAAGTTTCAGGTGACTGAG
GSTA1	Forward	AGGTATAGCAGATTTGGGTG
	Reverse	AAGACTTTTTCAAAGCAGG
GSTA2	Forward	CTATTGAGAGGAACAAGAGC
	Reverse	GCTTTGTTAAATGCTGTAC
GSTA3	Forward	ACCAATGGTTGAGATTGATG
	Reverse	TTAGGGCTCTCTCTTTATG
GSTA4	Forward	AAAGATTTAAGGGGTCACG
	Reverse	GAAATGCAGACAGGATATTAGG
GSTA5	Forward	AAAGTCTTAAAGAGCCACAG
	Reverse	GTAGTAGAAAAGTCCACCAG
GSTM1	Forward	CAATCTGCCCTACTTGATTG
	Reverse	GTCTGGTTCTCCAAAATGTC
GSTM2	Forward	AGATCACCTTTGTGGATTTT
	Reverse	GATGAAGTCCTCAGGTTTG
GSTM3	Forward	TTGAGGCTTTGGAGAAAATC
	Reverse	TGAAAAGAGCAAAGCAAGAG
GSTP1	Forward	TTCCAGTTCGAGGC
	Reverse	ATAGGCAGGAGGCTTTG
NQO1	Forward	AGTATCCACAATAGCTGACG
	Reverse	TTTGTGGTCTGTAGAAATG
GCLC	Forward	TTATTAGAGACCCACTGACAC
	Reverse	TTCTCAAATGGTCAGACTC
GCLM	Forward	CAATGATCCAAAAGAACTGC
	Reverse	CTCTACTTTTACAATGACCG
GSR	Forward	GACCTATTCACAGCTTTAC
	Reverse	CAACCACCTTTCTTCTTCTG
SLC7A11	Forward	GGTTATTCTATGTTGCGTCTC
	Reverse	AATAACAGCTGGTAGAGGAG
LAMP1	Forward	AGTGCTGCTGGACGAGAAC
	Reverse	GACCCTAAGCCAGAGAAAAG
LAMP2	Forward	TTCTGGTCTGCCTAGTCTCTG
	Reverse	ACAGTGCATGGTCTGAAAT
LC3B	Forward	GAATTCTCCACACCAAGTG
	Reverse	AAATAGTGAACCCATGCAA
SQSTM1	Forward	GAGTCCAGCACAGAGGAGA
	Reverse	AAGACAGATGGGTCCAGTCA
UVRAG	Forward	TGTCCTGCATAACAGCTTCA
	Reverse	GGCTTCTGCAGATCCAGTTA
WIPI1	Forward	TCTCAAGCTGGAACAGGTC
	Reverse	CTCTGTCGGAGAAAGTTCAA
BECN1	Forward	GCTGAGAGACTGGATCAGGA
	Reverse	ATTGTGCCAAACTGTCCACT
GABARAP	Forward	ACCAGGAACACCATGAAGAA
	Reverse	AGAGAGGCTGGAGAGAAAGC
GABARAPL1	Forward	TTATCTCACCCCTTCTTGG
	Reverse	GCCATCATGTAGCATTCTCTG
GABARAPL2	Forward	CTAGGTGCACCGTAACTGCT
	Reverse	CATGAGGACAATGCACAAA
ATG4A	Forward	GAGCAACTGGAGGATTTGA
	Reverse	TGGCTCAGTCATGATTGCTA
ATG4B	Forward	AGATTGGAGGTGCACAAA
	Reverse	ACGTATCGAAGACAGCAAGC

(Continued)

(Continued).

ATG4C	Forward	ATTGGTGGCAAACCTAAACA
	Reverse	TTGTACAGCTGGGATCCATT
ATG5	Forward	ATGCAGGGAACACTAAGCTG
	Reverse	TCTAGGGCATTGTAGGCTTG

Statistical analysis

Statistical analyses were performed using GraphPad Prism. The statistical significance of the differences between the groups was tested using t-test or two-way ANOVA. All experiments have been repeated a minimum of three times where samples were measured in technical triplicate.

Acknowledgements

The authors would like to thank members of the Bast laboratory for their discussion and suggestions. Flow cytometry studies were conducted in the Advanced Cytometry & Sorting Facility at South Campus at MD Anderson Cancer Center provided services for Flow cytometry studies. This work was supported by National Cancer Institute R01 CA266187 (RC Bast and Z Lu PIs), the MD Anderson Ovarian SPOREs P50 CA83639 (RC Bast and A Sood PIs) and P50 CA217685 (RC Bast and A Sood PIs), National Cancer Institute, Department of Health and Human Services, the Shared Resources of the MD Anderson CCSG grant NCI P30 CA 16672, the Cancer Prevention Research Institute of Texas RP140429 (RC Bast, PI); and generous donations from the Ann and Henry Zarrow Foundation, The Mossy Foundation, the Roberson Endowment, and Stuart and Gaye Lynn Zarrow. G.B. was supported by a CPRIT Training Award (RP210028), the HERA Ovarian Cancer Foundation, and the Mentored Investigator Award from the Ovarian Cancer Research Alliance.

Disclosure statement

No potential conflict of interest was reported by the author(s).

Funding

The work was supported by the Cancer Prevention and Research Institute of Texas [RP210028]; Cancer Prevention and Research Institute of Texas [RP140429]; National Cancer Institute [P30 CA 16672]; National Cancer Institute [R01 CA266187]; HERA Ovarian Cancer Foundation; MD Anderson Ovarian SPOREs [P50CA83639 and P50CA217685]; Ovarian Cancer Research Alliance [Mentored Investigator Award from].

ORCID

Gamze Bildik  <http://orcid.org/0000-0002-7596-2381>

Zhen Lu  <http://orcid.org/0000-0002-9596-0148>

References

- [1] Downward J. Ras signalling and apoptosis. *Curr Opin Genet Dev.* 1998;8(1):49–54. doi: 10.1016/S0959-437X(98)80061-0
- [2] Marshall C. How do small GTPase signal transduction pathways regulate cell cycle entry? *Curr Opin Cell Biol.* 1999;11(6):732–736. doi: 10.1016/S0955-0674(99)00044-7
- [3] Malumbres M, Barbacid M. RAS oncogenes: the first 30 years. *Nat Rev Cancer.* 2003;3(6):459–465. doi: 10.1038/nrc1097
- [4] Mukhopadhyay S, Vander Heiden MG, McCormick F. The metabolic landscape of RAS-Driven cancers from biology to therapy. *Nat Cancer.* 2021;2(3):271–283. doi: 10.1038/s43018-021-00184-x

- [5] Diaz-Padilla I, Malpica AL, Minig L, et al. Ovarian low-grade serous carcinoma: a comprehensive update. *Gynecol Oncol.* 2012;126(2):279–285. doi: [10.1016/j.ygyno.2012.04.029](https://doi.org/10.1016/j.ygyno.2012.04.029)
- [6] Kimmelman AC. Metabolic dependencies in RAS-Driven cancers. *Clin Cancer Res.* 2015;21(8):1828–1834. doi: [10.1158/1078-0432.CCR-14-2425](https://doi.org/10.1158/1078-0432.CCR-14-2425)
- [7] Pupo E, Avanzato D, Middonti E, et al. KRAS-Driven metabolic rewiring reveals novel actionable targets in cancer. *Front Oncol.* 2019;9:848. doi: [10.3389/fonc.2019.00848](https://doi.org/10.3389/fonc.2019.00848)
- [8] Kinsey CG, Camolotto SA, Boespflug AM, et al. Protective autophagy elicited by RAF→MEK→ERK inhibition suggests a treatment strategy for RAS-driven cancers. *Nat Med.* 2019;25(4):620–627. doi: [10.1038/s41591-019-0367-9](https://doi.org/10.1038/s41591-019-0367-9)
- [9] Bryant KL, Stalneck CA, Zeitouni D, et al. Combination of ERK and autophagy inhibition as a treatment approach for pancreatic cancer. *Nat Med.* 2019;25(4):628–640. doi: [10.1038/s41591-019-0368-8](https://doi.org/10.1038/s41591-019-0368-8)
- [10] Sutton MN, Lu Z, Li YC, et al. DIRAS3 (ARHI) blocks RAS/MAPK signaling by binding directly to RAS and disrupting RAS clusters. *Cell Rep.* 2019;29:3448–3459 e6. doi: [10.1016/j.celrep.2019.11.045](https://doi.org/10.1016/j.celrep.2019.11.045)
- [11] Nakamura H, Takada K. Reactive oxygen species in cancer: Current findings and future directions. *Cancer Sci.* 2021;112:3945–3952. doi: [10.1111/cas.15068](https://doi.org/10.1111/cas.15068)
- [12] Wu WL, Papagiannakopoulos T. The pleiotropic role of the KEAP1/NRF2 pathway in cancer. *Annu Rev Cancer Biol.* 2020;4:413–435. doi: [10.1146/annurev-cancerbio-030518-055627](https://doi.org/10.1146/annurev-cancerbio-030518-055627)
- [13] Nowosad A, Jeannot P, Callot C, et al. p27 controls Ragulator and mTOR activity in amino acid-deprived cells to regulate the autophagy-lysosomal pathway and coordinate cell cycle and cell growth. *Nat Cell Biol.* 2020;22(9):1076–1090. doi: [10.1038/s41556-020-0554-4](https://doi.org/10.1038/s41556-020-0554-4)
- [14] Liang J, Shao SH, Xu Z-X, et al. The energy sensing LKB1–AMPK pathway regulates p27kip1 phosphorylation mediating the decision to enter autophagy or apoptosis. *Nat Cell Biol.* 2007;9(2):218–224. doi: [10.1038/ncb1537](https://doi.org/10.1038/ncb1537)
- [15] Settembre C, Di Malta C, Polito VA, et al. TFEB Links Autophagy to Lysosomal Biogenesis. *Science.* 2011;332(6036):1429–1433. doi: [10.1126/science.1204592](https://doi.org/10.1126/science.1204592)
- [16] Napolitano G, Ballabio A. TFEB at a glance. *J Cell Sci.* 2016;129:2475–2481. doi: [10.1242/jcs.146365](https://doi.org/10.1242/jcs.146365)
- [17] Hennig P, Fenini G, Di Filippo M, et al. The pathways underlying the multiple roles of p62 in inflammation and cancer. *Biomedicines.* 2021;9(7):707. doi: [10.3390/biomedicines9070707](https://doi.org/10.3390/biomedicines9070707)
- [18] Komatsu M, Kurokawa H, Waguri S, et al. The selective autophagy substrate p62 activates the stress responsive transcription factor Nrf2 through inactivation of Keap1. *Nat Cell Biol.* 2010;12(3):213–223. doi: [10.1038/ncb2021](https://doi.org/10.1038/ncb2021)
- [19] Prior IA, Muncke C, Parton RG, et al. Direct visualization of Ras proteins in spatially distinct cell surface microdomains. *J Cell Bio.* 2003;160(2):165–170. doi: [10.1083/jcb.200209091](https://doi.org/10.1083/jcb.200209091)
- [20] Zhou Y, Gorfe AA, Hancock JF. RAS nanoclusters selectively sort distinct lipid headgroups and acyl chains. *Front Mol Biosci.* 2021;8:686338. doi: [10.3389/fmolb.2021.686338](https://doi.org/10.3389/fmolb.2021.686338)
- [21] Jeon S-M, Hay N. The dark face of AMPK as an essential tumor promoter. *Cell Logist.* 2012;2:197–202. doi: [10.4161/cl.22651](https://doi.org/10.4161/cl.22651)
- [22] Kimmelman AC, White E. Autophagy and tumor metabolism. *Cell Metab.* 2017;25(5):1037–1043. doi: [10.1016/j.cmet.2017.04.004](https://doi.org/10.1016/j.cmet.2017.04.004)
- [23] Guo JY, Teng X, Laddha SV, et al. Autophagy provides metabolic substrates to maintain energy charge and nucleotide pools in Ras-driven lung cancer cells. *Genes Dev.* 2016;30(15):1704–1717. doi: [10.1101/gad.283416.116](https://doi.org/10.1101/gad.283416.116)
- [24] Filomeni G, De Zio D, Cecconi F. Oxidative stress and autophagy: the clash between damage and metabolic needs. *Cell Death Differ.* 2015;22(3):377–388. doi: [10.1038/cdd.2014.150](https://doi.org/10.1038/cdd.2014.150)
- [25] Reczek CR, Chandel NS. The two faces of reactive oxygen species in cancer. *Annu Rev Cancer Biol.* 2017;1(1):79–98. doi: [10.1146/annurev-cancerbio-041916-065808](https://doi.org/10.1146/annurev-cancerbio-041916-065808)
- [26] Mauthe M, Orhon I, Rocchi C, et al. Chloroquine inhibits autophagic flux by decreasing autophagosome-lysosome fusion. *Autophagy.* 2018;14(8):1435–1455. doi: [10.1080/15548627.2018.1474314](https://doi.org/10.1080/15548627.2018.1474314)
- [27] Rebecca VW, Nicastrì MC, Fennelly C, et al. PPT1 promotes tumor growth and is the molecular target of chloroquine derivatives in cancer. *Cancer Discov.* 2019;9(2):220–229. doi: [10.1158/2159-8290.CD-18-0706](https://doi.org/10.1158/2159-8290.CD-18-0706)
- [28] Gray JP, Bildik GE, Sutton MN, et al. Abstract 3599: helical stapled peptides derived from DIRAS3 block KRAS dimerization and downstream MEK/ERK signaling in pancreatic and ovarian carcinomas. *Cancer Res.* 2022;82(12_Supplement):3599–3599. doi: [10.1158/1538-7445.AM2022-3599](https://doi.org/10.1158/1538-7445.AM2022-3599)
- [29] Bildik G, Liang X, Sutton MN, et al. DIRAS3: an imprinted tumor suppressor gene that regulates RAS and PI3K-driven cancer growth, motility, autophagy, and tumor dormancy. *Mol Cancer Ther.* 2022;21(1):25–37. doi: [10.1158/1535-7163.MCT-21-0331](https://doi.org/10.1158/1535-7163.MCT-21-0331)
- [30] Wu X, Liang L, Dong L, et al. Effect of ARHI on lung cancer cell proliferation, apoptosis and invasion in vitro. *Mol Biol Rep.* 2013;40(3):2671–2678. doi: [10.1007/s11033-012-2353-x](https://doi.org/10.1007/s11033-012-2353-x)
- [31] Yuan J, Luo RZ, Fujii S, et al. Aberrant methylation and silencing of ARHI, an imprinted tumor suppressor gene in which the function is lost in breast cancers. *Cancer Res.* 2003;63:4174–4180.
- [32] Ouyang J, Pan X, Hu Z. The role of aplysia ras homolog I in colon cancer cell invasion and adhesion. *Exp Ther Med.* 2017;14:5193–5199. doi: [10.3892/etm.2017.5122](https://doi.org/10.3892/etm.2017.5122)
- [33] Fernandez ML, DiMattia GE, Dawson A, et al. Differences in MEK inhibitor efficacy in molecularly characterized low-grade serous ovarian cancer cell lines. *Am J Cancer Res.* 2016;6:2235–2251.
- [34] De Thaye E, Van de Vijver K, Van der Meulen J, et al. Establishment and characterization of a cell line and patient-derived xenograft (PDX) from peritoneal metastasis of low-grade serous ovarian carcinoma. *Sci Rep.* 2020;10:6688. doi: [10.1038/s41598-020-63738-6](https://doi.org/10.1038/s41598-020-63738-6)
- [35] Gump JM, Thorburn A. Sorting cells for basal and induced autophagic flux by quantitative ratiometric flow cytometry. *Autophagy.* 2014;10(7):1327–1334. doi: [10.4161/auto.29394](https://doi.org/10.4161/auto.29394)